

Solution of a multi-dimensional batch crystallization model with fines dissolution using CE/SE method

Saima Noor¹, Shamsul Qamar²

¹ Department of Mathematics, COMSATS Institute of Information Technology, University road, Tobe Camp, Abbottabad, Pakistan

² Department of Mathematics, COMSATS Institute of Information Technology, Park road, Chak Shahzad Campus, Pakistan

saimmanoor@gmail.com

Abstract: This article is concerned with the numerical investigation of two-dimensional population balance models for batch crystallization processes with fines dissolution. In batch crystallization, dissolution of smaller unwanted nuclei below some critical size is of vital importance as it improves the quality of the product. The crystals growth rates for both size-independent and size-dependent cases are considered. Moreover, a delay in the recycle pipe is also included in the model. The space-time conservation element and solution element method, originally derived for non reacting flows, is used to solve the resulting model. This scheme has already been applied to a range of PDE's, mainly in the area of Fluid mechanics. The CE/SE method has been successfully applied to disciplines other than it originated from, this distinguishing feature confirms the method's robustness and generality. The numerical results in this article demonstrate the excellent performance of proposed numerical schemes in solving the current physical problem.

[Noor S, Qamar S. **solution of a multi-dimensional batch crystallization model with fines dissolution using CE/SE method.** *Life Sci J* 2014;11(2s):69-78]. (ISSN:1097-8135). <http://www.lifesciencesite.com>. 13

Keywords: Population balances, batch process, crystallization, fines dissolution, multi-dimensional problems, space-time CE/SE method.

1. Introduction

Crystallization is a very important unit operation, often used to produce solids from liquids. It has a wide range of speciality applications in chemical, pharmaceutical, material, and semiconductors industries. The process is proficient to provide high purity products and offers a potential to adjust the operating conditions for achieving the desired product properties. Its advantages such as its high product purity and low operating costs, make it more desirable as compared to other separation processes like extraction and distillation. It is important to understand and optimize the crystallization process for improving the product quality and for minimizing the production costs. This goal can be achieved by modeling and developing advanced control algorithms that can be implemented for online optimization of crystal size distribution. An accurate simulation of the distribution can be challenging as the distribution can extend many orders of magnitude in size and time.

In batch crystallization process, dissolution of small crystals (fines dissolution) can improve the quality of a product. The dissolution appears when the solution with crystals already formed is warmed up, taking place as a diminution in the CSD. The dissolution and the crystallization are being considered as the opposite processes to each other. Normally, large size crystals are of more interest in the industry. The fine dissolution reduces undesirable small crystals and helps in achieving the desired CSD.

Furthermore, it facilitates downstream processes like filtration.

Population balance based modeling is considered to be the most useful modeling approach for describing crystallization process along with several other chemical engineering processes. The Theory of population balances begins in 1960 when Hulburt and Katz [1] as well as Randolph and Larson [2] introduced them in the field of chemical engineering. Their wide range of application in industry provoked the researchers to get high interest in the solution of PBEs. Population balance equations are hyperbolic partial differential equations. Analytical solutions are possible only for a limited number of simple problems, which is why researchers have invested a lots of efforts to develop appropriate numerical schemes. With the passage of time, several numerical schemes were developed for Population balance models such as method of moments Marchisio et al. [3] and Barret et al. [4], the method of characteristic Kumar and Ramkrishna [5] Qamar and Warnecke [6], the method of weighted residuals Singh [7], the Monte Carlo method Shah et al. [8], Maisel et al. [9], Song [10], finite difference scheme Kumar and Ramkrishna [11], and the high resolution finite volume schemes Gunawan et al. [12], Qamar et al. [13], Qamar et al. [14].

In this article, a model for the simulation of a one and two-dimensional batch crystallization process with fines dissolution is derived. A simplified

dynamic model of ideally mixed batch crystallizer is considered here. It is assumed that fines completely dissolve at the end of recycle pipe attached to the crystallizer (see Figure (1)). The crystal growth rates can be size-dependent or size-independent and a delay in the recycle pipe is also integrated in the model. The space-time conservation element and solution element method is implemented for solving the resulting model. The CE/SE method originally developed by Gunawan et al. [15] is a new numerical frame work for solving conservation laws. Numerous striking features of CE/SE method such as extremely low numerical dissipation and simplicity of construction makes the CE/SE method very promising for CFD simulation.

This paper is organized as follows. In Section 2, two-dimensional batch crystallization model is presented. In Section 5, two-dimensional CE/SE scheme is derived. In Section 6, numerical test problems are presented. Finally, Section 7 gives conclusions and remarks.

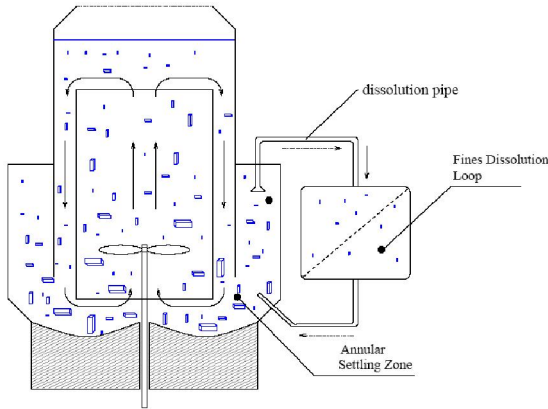


Figure 1: Single batch process setup with fines dissolution

2. Two dimensional batch crystallization with fines dissolution

In this section, we give two-dimensional mathematical model for the simulation of a batch crystallizer. In the two-dimensional case, the evolution of CSD $n(t, x, y) \geq 0$ is given as:

$$\frac{\partial n(t, x, y)}{\partial t} + \frac{\partial [G_1(t, x)n(t, x, y)]}{\partial x} + \frac{\partial [G_2(t, y)n(t, x, y)]}{\partial y} = -\frac{\dot{V}}{V_{crz}} h(x, y)n(t, x, y) + B_0(t)\delta(x - x_0, y - y_0), \quad (1)$$

$$n(0, x, y) = n_0(x, y), \quad (t, x, y) \in P_+^3, \quad (2)$$

where $P_+ := (0, \infty)$. Here, $n_0(x, y) \in P_{\geq 0}^2$ denotes the CSD of seed crystals added at the

beginning of the batch process, $G_1(t, x) \geq 0$ and $G_2(t, y) \geq 0$ are the crystals growth rates along the characteristic directions x and y , $B_0(t) \geq 0$ is the nucleation rate at minimum crystal size (x_0, y_0) , and δ is the Dirac delta distribution. Moreover, V_{crz} is volume of the crystallizer and \dot{V} is volumetric flow rate. The death function $h(x, y)$ describes the dissolution of small particles below some critical size. The ij th moment of CSD is defined as:

$$\mu_{i,j}(t) = \iint_{0,0}^{\infty,\infty} x^i y^j n(t, x, y) dx dy, \quad i, j = 0, 1, 2, \dots \quad (3)$$

Balance law for the liquid phase yields an ordinary differential equation (ODE) for the solute mass of the form:

$$\frac{dm(t)}{dt} = \dot{m}_{in}(t) - \dot{m}_{out}(t) - \rho_c \iint_{0,0}^{\infty,\infty} \left(G_1(t, x) \frac{\partial V_c}{\partial x} + G_2(t, y) \frac{\partial V_c}{\partial y} \right) n(t, x, y) dx dy. \quad (4)$$

Here, V_c represents the volume of a single crystal and ρ_c is a crystal density. Due to fines dissolution this equation has two mass fluxes. The inner and outer fluxes are defined as:

$$\dot{m}_{out}(t) = w(t)\rho_{solu}(T)\dot{V}, \quad (5)$$

$$\dot{m}_{in}(t) = \dot{m}_{out}(t - t_p) + \frac{\rho_c \dot{V}}{V_{crz}} \iint_{0,0}^{\infty,\infty} V_c h(x, y) n(t - t_p, x, y) dx dy - \rho_c V_c(x_0, y_0) B_0(t - t_p), \quad (6)$$

The expressions for size dependent growths are given as follows:

$$G_1(t, x) = k_{g_1} [S(t) - 1]^{\mathcal{G}_1} (1 + \alpha_1 x)^{\alpha_2} := g_1(t) g_2(x), \quad (7)$$

$$G_2(t, y) = k_{g_2} [S(t) - 1]^{\mathcal{G}_2} (1 + \alpha_3 y)^{\alpha_4} := g_3(t) g_4(y), \quad (8)$$

where k_{g_1} and k_{g_2} are the growth rates constant. The exponents \mathcal{G}_1 and \mathcal{G}_2 denote the growths order and $\alpha_1, \alpha_2, \alpha_3, \alpha_4$ are constants representing the size-dependency. The nucleation is defined as:

$$B_0(t) = k_b [S(t) - 1]^b \iint_{0,0}^{\infty,\infty} V_c n(t, x, y) dx dy, \quad (9)$$

b is nucleation rate constant and the exponent b gives the nucleation order. The model reduces to a batch crystallization model without fines dissolution when the first term on the right hand side of (1) and

the first two terms on the right-hand side of (4) are zero. Then equations (5) and (6) are not required.

3. The two dimensional CE/SE method

A detailed discussion on the derivation of two-dimensional CE/SE method is given in Ref. [16] as well as Ref. [17]. Here, we give a brief overview of this scheme. The equation of the two-dimensional batch crystallization model given in equation (1) can be re written as:

$$\frac{\partial w}{\partial t} + \frac{\partial f}{\partial x} + \frac{\partial g}{\partial y} = P \tag{10}$$

Here $w = n(t,x,y)$, $f = G_1(t,x)n(t,x,y)$, $g = G_2(t,y)n(t,x,y)$ and $Q = \frac{\dot{V}}{V_{crz}}h(x,y)n(t,x,y) + B_0(t)\delta(x-x_0, y-y_0)$. Assume that t , x and y are the coordinates of a three-dimensional Euclidean space E_3 . The integral representation of Eq. (10) is:

$$\oint_{s(V)} h \cdot d = 0 \tag{11}$$

Here $h = [w, f, g, -Q]^T$ represents the current density vectors in E_3 and $s(V)$ is the boundary of an arbitrary space-time domain V .

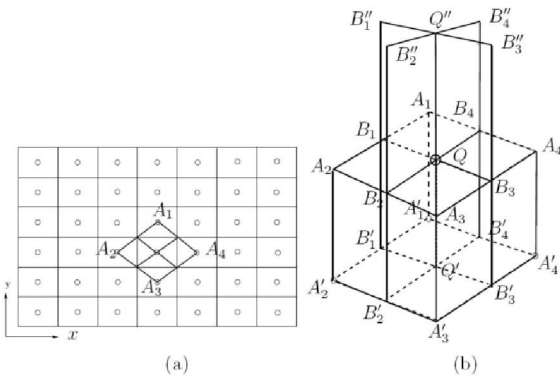


Figure 2: Space-time geometry of the modified CE/SE method: (a) representative grid points in x-y plane, (b) the definitions of CE and SE.

The whole domain is divided into non-overlapped uniform rectangular cells as given in Figure (2). The centroid of each cell is denoted by a circle symbol that also represents the grid point in this CE/SE method, for instance point Q in Figure 2(b). The set of these points is denoted by Ω . In contrast to the original CE/SE method, only one conservation element (CE) and associated one solution element (SE) belong to each element. =150,0mm Space-time geometry of the modified CESE method: (a)

representative grid points in x-y plane, (b) the definitions of CE and SE.

In Figure (2)(b), the grid points Q, A_1, A_2, A_3 and A_4 are lying at time level $t = t^n$ at which the new numerical solutions of flow variables are to be calculated. The points Q', A'_1, A'_2, A'_3 and A'_4 are the corresponding points at time level $t = t^{n-1/2}$ and the points Q'', B''_1, B''_2, B''_3 and B''_4 are located at time level $t = t^{n+1/2}$. The same rule is applied to all mesh points for denoting the time levels. The SE associated to point Q is defined by the union of one horizontal plane segment $A_1A_2A_3A_4$ and two vertical plane segments $B'_1B'_2B'_3B'_4$ and $B''_1B''_2B''_3B''_4$. The CE associated to point Q is given by the cylinder $A_1B_1A_2B_2A_3B_3A_4B_4$ $A'_1B'_1A'_2B'_2A'_3B'_3A'_4B'_4$. The centroid Q of the top surface of this CE, denoted by polygon $A_1B_1A_2B_2A_3B_3A_4B_4$ is taken as the solution point. All the variables and their spatial derivative are stored at point Q denoting the set of solution points Ω .

Inside each SE, the flow variables are assumed smooth and the structure of the flow solution is discretized by a prescribed function. Following Chang's approach, the distribution of W , k and g can be approximated by first-order Taylor expansions about point Q . In other words, for any $(t, x, y) \in SE(Q)$, $w(t, x, y)$, $f(t, x, y)$ and $g(t, x, y)$ are approximated as:

$$w^*(t, x, y) = (w_t)_Q(t-t^n) + (w)_Q + (w_x)_Q(x-x_Q) + (w_y)_Q(y-y_Q), \tag{12}$$

$$f^*(t, x, y) = (f_t)_Q(t-t^n) + (f)_Q + (f_x)_Q(x-x_Q) + (f_y)_Q(y-y_Q), \tag{13}$$

$$g^*(t, x, y) = (g_t)_Q(t-t^n) + (g)_Q + (g_x)_Q(x-x_Q) + (g_y)_Q(y-y_Q). \tag{14}$$

Here t^n, x_Q, y_Q are the space-time coordinates of Q . The variables w, w_t, w_x and w_y on the right hand side of Eq. (12) are the discretized variables. If these variables are available, the flow solution structure within SE is fully specified. However, the above variables are not completely independent. By employing Eq. (10), we obtain:

$$(w_t)_Q = -(f_x)_Q - (g_y)_Q - (P)_Q. \tag{15}$$

To derive the scheme, the continuous space-time flux vector $h(t, x, y)$ is replaced by a discrete one $h^*(t, x, y) = [w^*(t, x, y), f^*(t, x, y), g^*(t, x, y)]^T$ (16)

and the Eq. (11) by its discrete counterpart $\oint_{S(CE(Q))} h^* \cdot dS = 0$. (17)

On substituting Eqs. (12)-(16) into Eq. (17), the following algebraic equation can be obtained:

$$(w)_Q^n = \left(\sum_{l=1}^4 R^l \right) / S + \frac{s \Delta t}{2} (Q)_Q^{n-1/2}, \quad (18)$$

where

$$R^{(l)} = s_q^{(l)} \begin{bmatrix} (w)_{A_l}^{n-1/2} + (x_q^{(l)} - x_{A_l})(w_x)_{A_l}^{n-1/2} \\ + (y_q^{(l)} - y_{A_l})(w_y)_{A_l}^{n-1/2} \\ (f)_{A_l}^{n-1/2} + (x_m^{(l)} - x_{A_l})(f_x)_{A_l}^{n-1/2} \\ + (y_m^{(l)} - y_{A_l})(f_y)_{A_l}^{n-1/2} \\ + \Delta t/4 \cdot (f_t)_{A_l}^{n-1/2} - (w_x)_{A_l}^{n-1/2} \\ (g)_{A_l}^{n-1/2} + (x_m^{(l)} - x_{A_l})(g_x)_{A_l}^{n-1/2} \\ + (y_m^{(l)} - y_{A_l})(g_y)_{A_l}^{n-1/2} \\ + \Delta t/4 \cdot (g_t)_{A_l}^{n-1/2} - (w_y)_{A_l}^{n-1/2} \end{bmatrix} \quad (19)$$

for $l=1,2,3,4$ indicating the spatial flux contribution from the four neighboring points. Here $(x_q^{(l)}, y_q^{(l)})$ and $s_q^{(l)}$ are the spatial coordinates of the centroid and the area of the four neighboring quadrilaterals $A_1B_1QB_4$, $A_2B_2QB_1$, $A_3B_3QB_2$ and $A_4B_4QB_3$. Moreover, $n_m^{(l)} = [n_{mx}^{(l)}, n_{my}^{(l)}, 0]^T$ represent the eight surface vectors of the eight lateral planes: $A_1'B_4'A_1B_4$, $A_1'B_1'A_1B_1$, $A_2'B_1'A_2B_1$, $A_2'B_2'A_2B_2$, $A_3'B_2'A_3B_2$, $A_3'B_3'A_3B_3$, $A_4'B_3'A_4B_3$ and $A_4'B_4'A_4B_4$. Note that, the surface vector is defined as the unit outward normal vector (outward from the interior of the CE) multiplied by its area. Finally, S is the area of the polygon $A_1B_1A_2B_2A_3B_3A_4B_4$ that also represents the top surface of the present CE. Because all flow conditions at the $n-1/2$ time level are known, Eqs. (18) and (19) represent an explicit method for calculating w^n at point Q .

To calculate $(w_x)_Q$ and $(w_y)_Q$, a central difference-type reconstruction procedure is employed. Due to Taylor series:

$$(w')_{A_l}^n = (w)_{A_l}^{n-1/2} + \frac{\Delta t}{2} (w_t)_{A_l}^{n-1/2}, \quad l=1,2,3,4. \quad (20)$$

This predicted value actually represents a linear expansion in time. By using the values of $(w_m)_{A_1}^n$, $(w_m)_{A_2}^n$ and $(w_m)_Q^n$, the first pair of spatial derivatives of flow variables can be obtained, i.e., $w_x^{(1)}$, $w_y^{(1)}$ at point Q :

$$w_x^{(1)} = D_x/D, \quad w_y^{(1)} = D_y/D, \quad (21)$$

where

$$D = \begin{bmatrix} \Delta x_1 & \Delta y_1 \\ \Delta x_2 & \Delta y_2 \end{bmatrix}, \quad D_x = \begin{bmatrix} \Delta w^{(1)} & \Delta y_1 \\ \Delta w^{(2)} & \Delta y_2 \end{bmatrix}, \quad D_{my} = \begin{bmatrix} \Delta x_1 & \Delta w^{(1)} \\ \Delta x_2 & \Delta w^{(2)} \end{bmatrix}, \quad (22)$$

$$\Delta x_l = (x_{A_l} - x_Q), \quad \Delta y_l = (y_{A_l} - y_Q), \quad \Delta w^{(l)} = ((w)_{A_l}^n - (w)_Q^n). \quad (23)$$

Similarly, the solutions at A_2 , A_3 and Q gives the second pair $w_x^{(2)}$, $w_y^{(2)}$, the solutions at A_3 , A_4 and Q gives the third pair $w_x^{(3)}$, $w_y^{(3)}$ while the solutions at A_4 , A_1 and Q gives the fourth pair $w_x^{(4)}$, $w_y^{(4)}$. Finally, re-weighting procedure is used to calculate w_x and w_y at Q as follows [15,16,18]:

$$(w_{kx})_Q^n = \begin{cases} 0, & \text{if } \theta_{kl} = 0, \quad (l=1,2,3,4), \\ \sum_{m=1}^4 [(w_k^{(m)})^\alpha w_{kx}^{(m)}] / \sum_{m=1}^4 (w_k^{(m)})^\alpha, & \text{otherwise,} \end{cases} \quad (24)$$

$$(w_{ky})_Q^n = \begin{cases} 0, & \text{if } \theta_{kl} = 0, \quad (l=1,2,3,4), \\ \sum_{m=1}^4 [(w_k^{(m)})^\alpha w_{ky}^{(m)}] / \sum_{m=1}^4 (w_k^{(m)})^\alpha, & \text{otherwise,} \end{cases} \quad (25)$$

where

$$w_k^{(m)} = \prod_{l=1, l \neq m}^4 \theta_{kl}, \quad \theta_{kl} = \sqrt{(w_{kx}^{(l)})^2 + (w_{ky}^{(l)})^2}. \quad (26)$$

In Eqs. (24) and (25), the value of constant α can be either 1 or 2. The Eqs. (24) and (25) are simple and effective to suppress spurious oscillations near the shocks. This concludes the derivation of two-dimensional CE/SE method on rectangular grids.

4. Numerical test problem

4.1 One dimensional case study

In this section we have considered a numerical test problem in order to validate our numerical schemes for the given model. The initial data is given as:

$$n(0, x) = \frac{m_{seeds}}{k_v \rho_c \mu_3(0) \sqrt{2\pi\sigma}} \exp\left(-\frac{(x-\bar{x})^2}{2\sigma^2}\right), \quad (27)$$

where $x_0 = 0$ and $x_{max} = 0.005$ are the minimum and maximum crystal sizes respectively. The interval $[0, x_{max}]$ is divided into 300 grid points and the simulation time is taken to be 800 minutes. The temperature of the crystallizer was kept constant at $33^\circ C$. The kinetic parameters are given in Table (1).

Table 1: Parameters for the test problem 1

Description	Symbols	Value	Unit
Growth rate constant	k_g	$1.37 \cdot 10^{-5}$	m/min
Growth rate exponent	g_1	0.73	—
Nucleation rate constant	k_b	$3.42 \cdot 10^7$	$1/m^3 min$
Nucleation rate exponent	b	2.35	—
Density of crystals	ρ_c	1250	kg/m^3
Volume shape factor	k_v	0.029	—
Initial solute concentration (mass)	$m(0)$	0.09915	kg
Saturated mass fraction	w_{sat}	0.090681	—
Mass of seeds	m_{seeds}	$2.5 \cdot 10^{-3}$	kg
Mass of solvent	m_{solv}	0.8017	kg
Density of solution	ρ_{solu}	1000	kg/m^3
Constant (Eq.(28))	σ	$3.2 \cdot 10^{-4}$	m
Constant (Eq. (28))	\bar{x}	$1.4 \cdot 10^{-3}$	M
volume of the crystallizer	V_{crz}	$10^{-3} \cdot 10^{-3}$	m^3
volumetric flow rate	\dot{V}	2×10^{-5}	m^3/min
volume of the pipe	V_p	2.4×10^{-4}	m

The death function $h(x)$ is defined as:

$$h(x) = \frac{1}{\sqrt{2\pi}\sigma_1} \exp\left(-\frac{x}{\alpha\sigma_1}\right)^2, \sigma_1 = \frac{1}{\sqrt{2\pi}\sigma n_{max}} \quad (28)$$

where $\alpha = 0.0011547$ and $n_{max} = 0.6$. Final crystal size distribution for size-independent growth

and size-dependent growth is shown in figure (5). In this figure final CSD for the model without fines dissolution, fines dissolution with and without time delay are compared. From figure it can be seen that in case of without fines dissolution there is a large number of small unwanted nuclei which can affect the product quality, while the dissolution unit dissolves the small crystal below some critical size and reduces the number of small crystals in the crystallizer. In case of fines dissolution without time delay small crystals are dissolve back as soon as they are introduced in the solution, so its effect on crystal growth rate is negligible. On the other hand, fines dissolution with time delay permits nuclei to grow for a certain time and the concentrated solution from dissolution unit get back to the crystallizer with a time delay. As a result the seed crystals grow at a faster rate. Furthermore, figures (6) and (7) gives a comparison of the proposed scheme and the finite volume Koren scheme for fines dissolution with and without time delay for both size-independent and size dependent growth rates. The numerical results for both the schemes are almost overlapping. However the current scheme gives better results for the proposed model.

4.2 Two dimensional case study

In order to validate our numerical schemes for the given model, we consider the following numerical test problem. The initial data and other parameter in this problem are chosen for numerical purpose and are not belonging to any experimental setup. The initial data are taken as (see Figure (4)):

$$n(0, x, y) = \frac{m_{seeds}}{V_s(0)\sqrt{2\pi}\sigma} \exp\left(\frac{-(x-\bar{x})^2 - (y-\bar{y})^2}{2\sigma^2}\right), \quad (29)$$

where

$$V_s(0) = \iint_{00}^{\infty\infty} \frac{V_c}{\sqrt{2\pi}\sigma} \exp\left(\frac{-(x-\bar{x})^2 - (y-\bar{y})^2}{2\sigma^2}\right) dx dy. \quad (30)$$

We assume the rectangular shaped crystals of volume $V_c = x^2 y$, where x is the width and y is the length of the crystal. Let $(x_0, y_0) = (0, 0)$ and $(x_{max}, y_{max}) = (0.0025m, 0.005m)$. The interval $[0, x_{max}] \times [0, y_{max}]$ is subdivided into 200×400 grid points and the final simulation time is 600 minutes. In the case of size-dependent growth rates we choose $\alpha_1 = 150$, $\alpha_3 = 300$, while $\alpha_2 = 1 = \alpha_4$ in all cases. For size-independent case $\alpha_1 = 0 = \alpha_3$. The kinetic parameters and other constants are given in Table (2).

The crystallizer was kept at a constant temperature of 33°C

Table 2: Parameters for the test problem 2

Description	Symbols	Value	Unit
Growth rate constant	k_{g1}	$0.68 \cdot 10^{-5}$	m/min
Growth rate constant	k_{g2}	$1.37 \cdot 10^{-5}$	m/min
Growth rate exponent	g_1	0.73	—
Growth rate exponent	g_2	0.73	—
Nucleation rate constant	k_b	$3.42 \cdot 10^7$	$1/m^3 \cdot min$
Nucleation rate exponent	b	2.35	—
Density of crystals	ρ_c	1250	kg/m^3
Initial solute concentration (mass)	$m(0)$	0.09915	Kg
Saturated mass fraction	w_{sat}	0.090681	—
Mass of seeds	m_{seeds}	$2.5 \cdot 10^{-3}$	kg
Mass of solvent	m_{solv}	0.8017	kg
Density of solution	ρ_{solu}	1000	kg/m^3
Constant (Eq. (29))	σ	$2.1 \cdot 10^{-4}$	m
Constant (Eq. (29))	\bar{x}	$7.0 \cdot 10^{-4}$	m
Constant (Eq. (29))	\bar{y}	$1.0 \cdot 10^{-3}$	m
volume of the crystallizer	V_{crz}	10^{-3}	m^3
volumetric flow rate	\dot{V}	$2 \cdot 10^{-5}$	m^3/min
volume of the pipe	V_p	$2.4 \cdot 10^{-4}$	m

The following death function $h(x,y)$ is assumed in this problem (see Figure (3)):

$$h(x,y) = \begin{cases} 0.6, & \text{if } (0,0) \leq (x,y) \leq (2 \times 10^{-4}, 4 \times 10^{-4}), \\ 0, & \text{otherwise.} \end{cases} \quad (31)$$

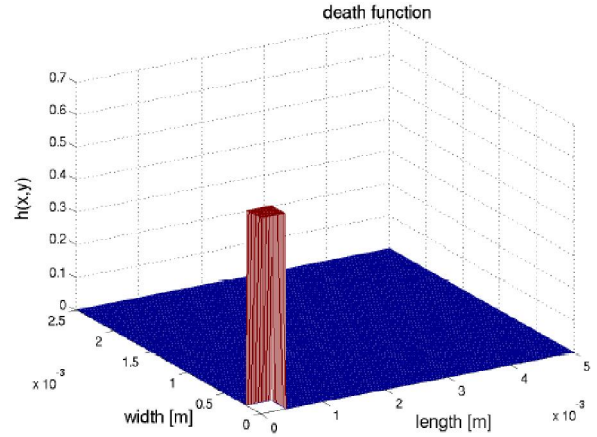


Figure 3: Death function $h(x,y)$

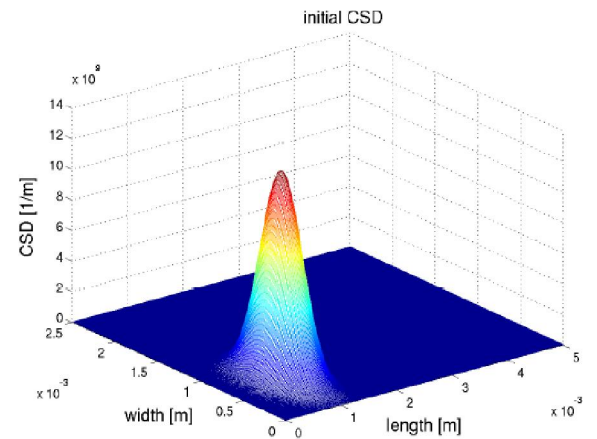
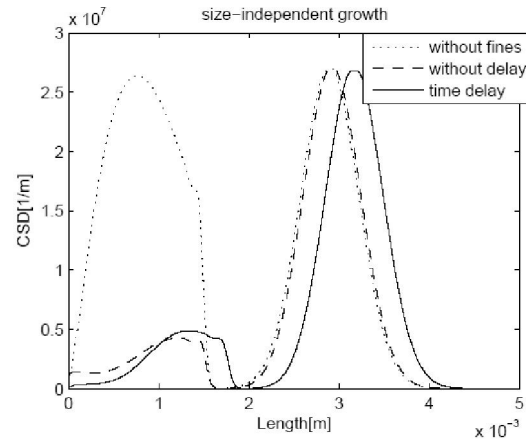


Figure 4: Initial CSD



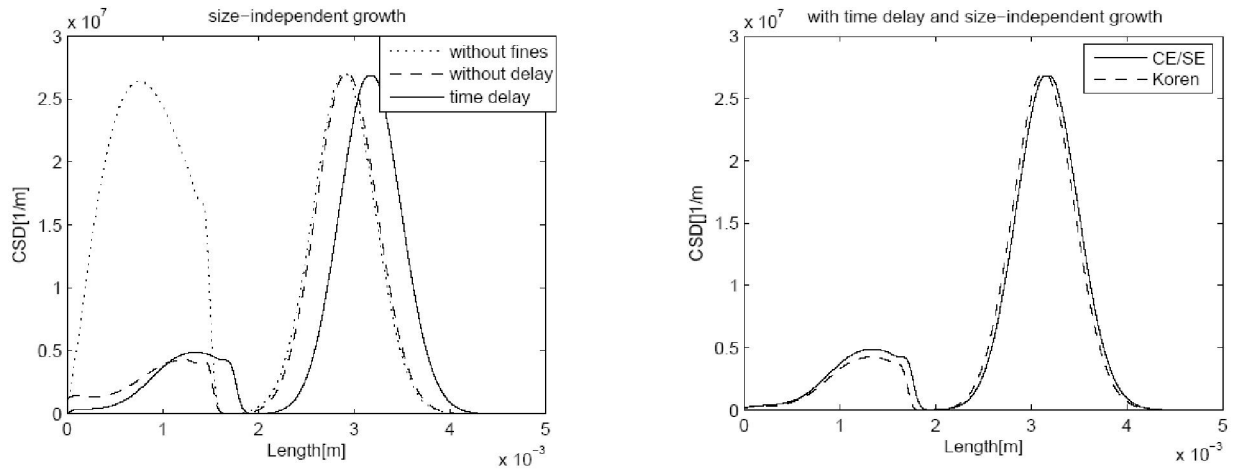


Figure 5: Top: Comparison of without fines dissolution, fines dissolution with and without time delay for size independent growth rate. Bottom: size dependent growth rate

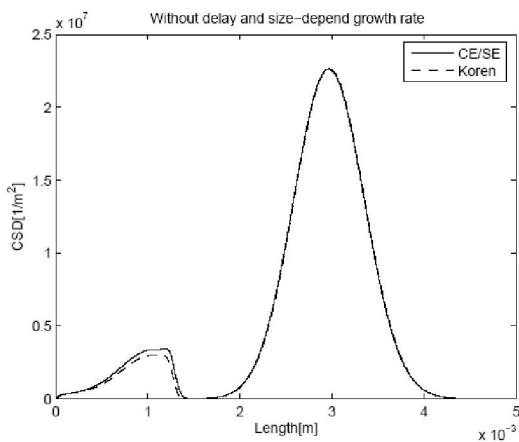
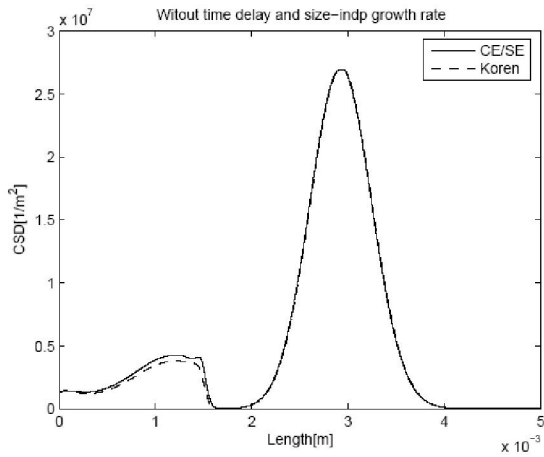


Figure 6: Top: Comparison of CE/SE and Koren for without time delay and size independent growth. Bottom: size dependent growth rate.

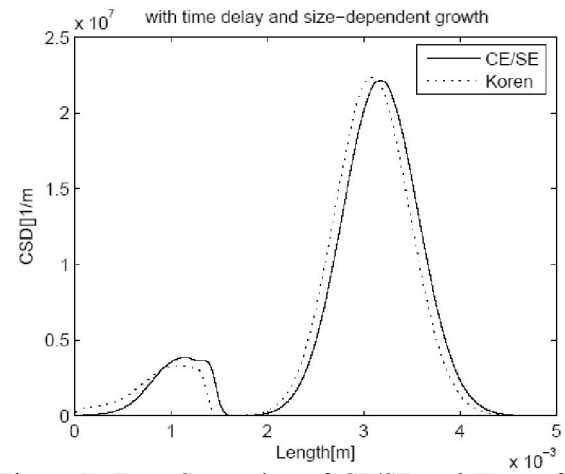
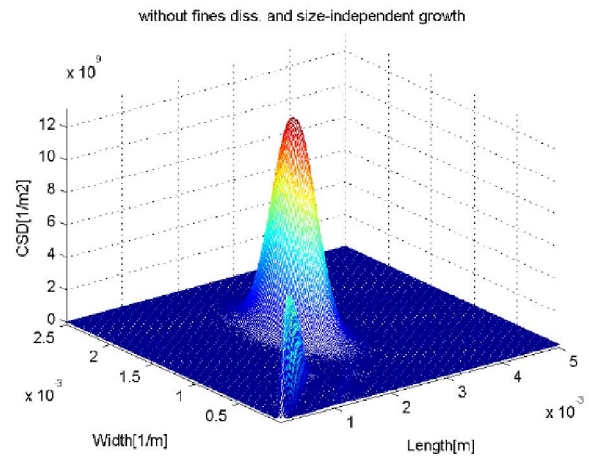


Figure 7: Top: Comparison of CE/SE and Koren for time delay and size independent growth. Bottom: size dependent growth rate.



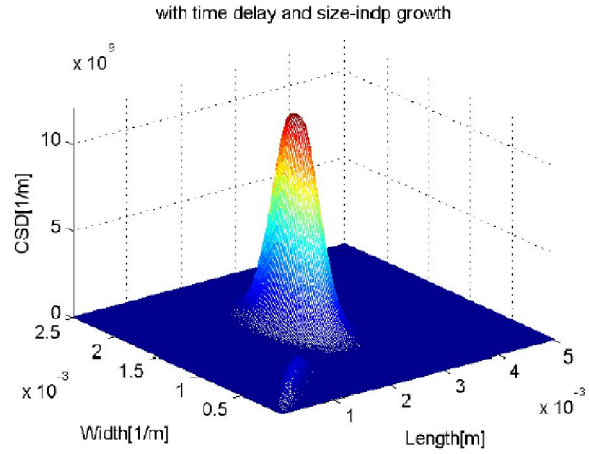
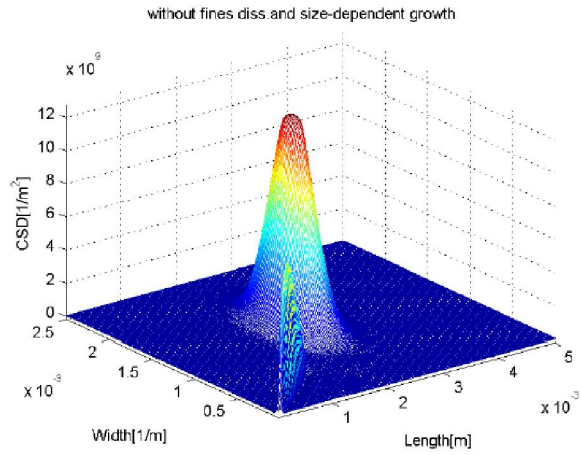


Figure8: Top: 3D plots for size independent and size dependent growth rate.

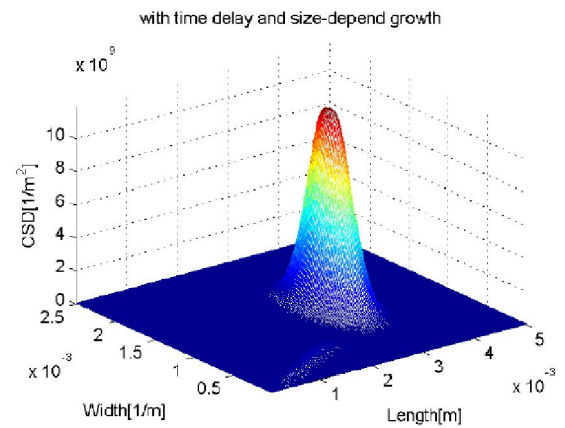
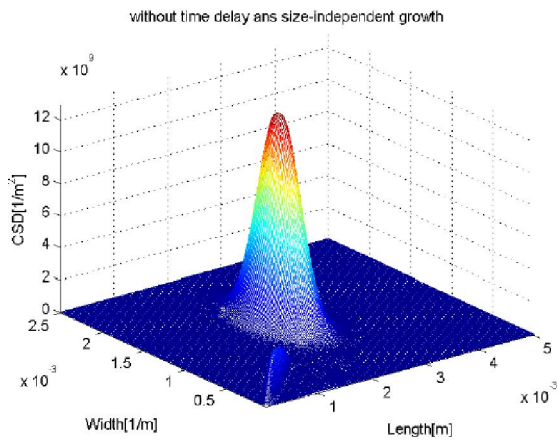


Figure 10: Top: 3D plots of fines dissolution with time delay for both size independent and size dependent case.

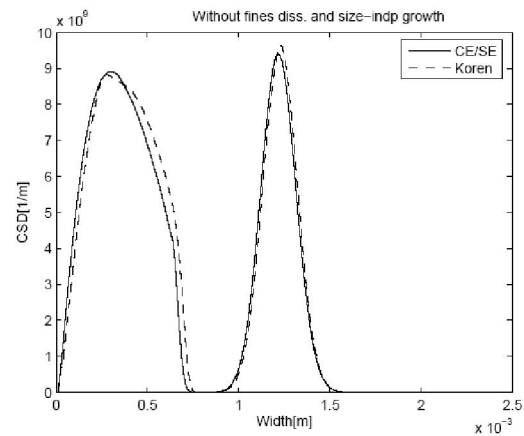
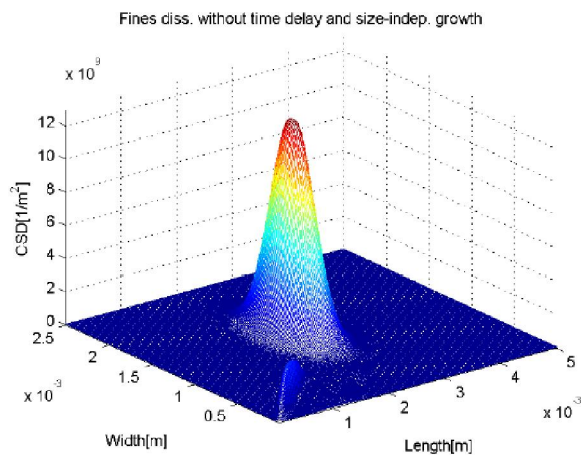


Figure 9: Top: 3D plots of fines dissolution without time delay for both size independent and size dependent case.

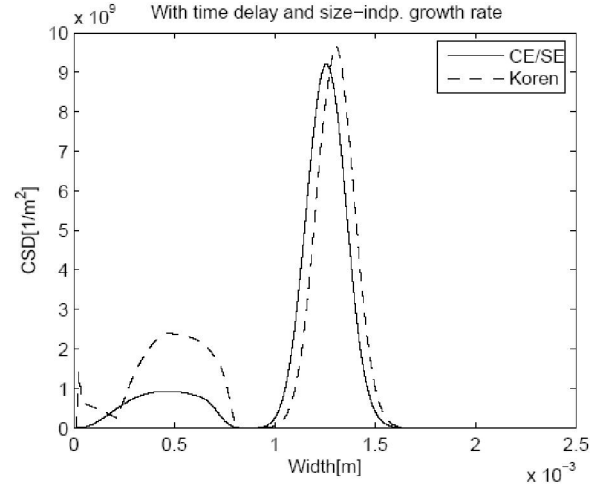
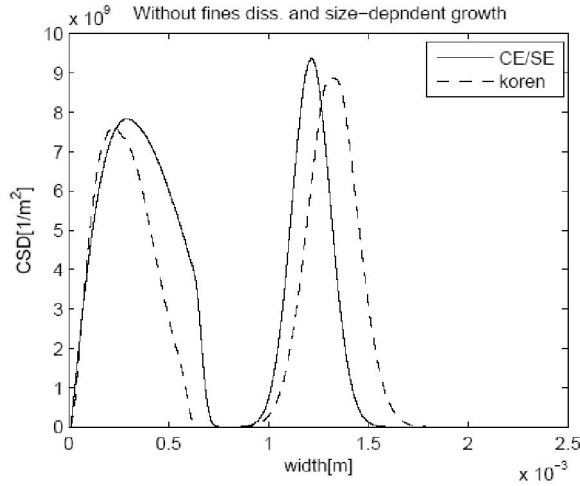


Figure 11: Top: Comparison of CE/SE and Koren for size independent growth. Bottom: size dependent.

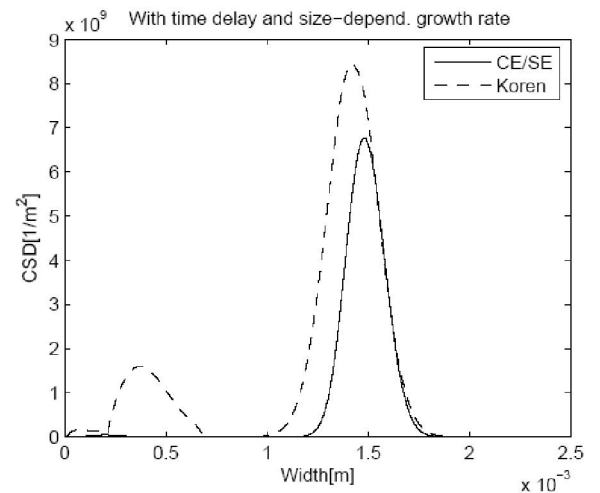
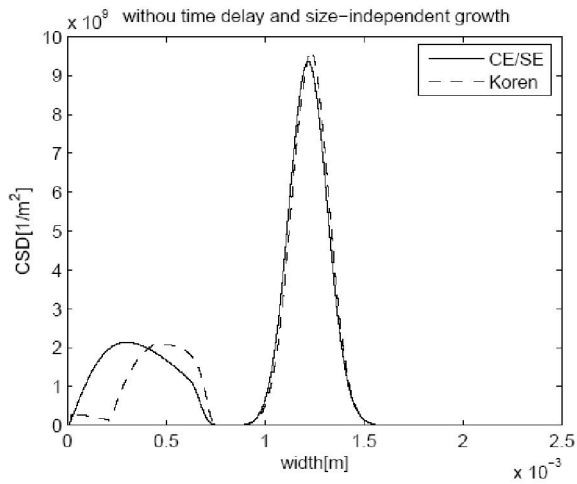


Figure 13: Top: Comparison of CE/SE and Koren for time delay and size independent growth. Bottom: size dependent.

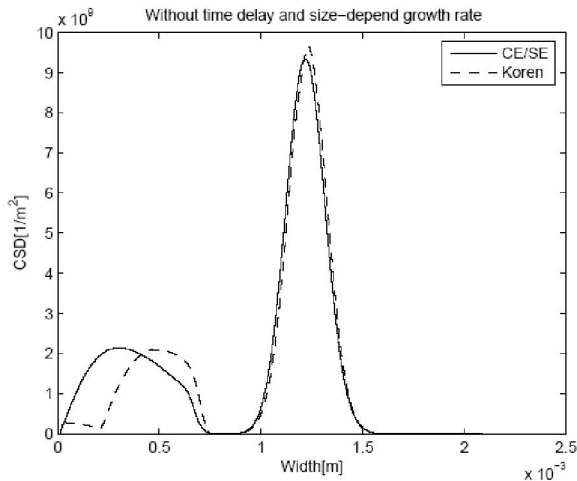


Figure 12: Top: Comparison of CE/SE and Koren for without delay and size independent growth. Bottom: size dependent.

In Figures (8) to (10) the final CSDs from the CESE method are given. In these figures, the three dimensional plots of final CSDs without fines dissolution and with fines dissolution as well with and without ($t_p = 0$) time delay are compared. Both size-independent and size-dependent growth cases are considered in this figure. Moreover, Figure (11) to (13) gives the comparison of the proposed CE/SE method and the High resolution Koren scheme. In these figures, the one-dimensional plots of CSDs along the line $x = 2y$ are given for without fines dissolution and with fines dissolution (with and without time delay). Both size independent and size dependent cases are considered.

5. Conclusion

In this paper, a mathematical model for two-dimensional batch crystallization process with fines dissolution was derived. From the case study it was observed that the dissolution of smaller nuclei below some critical size helps in improving the product quality. Crystals growth rates were considered to be both size-independent and size-dependent. Moreover, a delay in the recycle pipe was also incorporated in the model. The space time conservation element and solution element method, originally derived for non-reacting flows, was used to solve the resulting model. These schemes have already been applied to a range of PDE's, mainly in the area of Fluid mechanics. The numerical results show excellent performance of proposed numerical schemes for solving the current model.

Corresponding Author:

Dr. Saima Noor

Department of Mathematics

COMSATS Institute of Information Technology,

Abbottabad, Pakistan

E-mail: saimmanoor@gmail.com

References

- Hulburt, H. M., Katz, S. Some problems in particle technology. *Chem. Eng. Sci.* 1964:19: 555-574.
- Randolph, A. D., Larson, M. A. Theory of particulate processes, second edition, Academic Press. 1988.
- Marchisio, D. L., Vigil, R. D., Fox, R. O. Quadrature method of moments for aggregation-breakage processes. *J. Colloid Interface Sci.* 2003: 258: 322-334.
- Barret, J. C., Jheeta, J. S. Improving the accuracy of the moments method for solving the aerosol general dynamic equation. *J. of Aerosol. Sci.* 1996:27: 1135-1142.
- Kumar, S., Ramkrishna, D. On the solution of population balance equations by discretization -I. A fixed Pivot technique. *Chem. Eng. Sci.* 1996:51: 1311-1332.
- Qamar, S., Warnecke, G. Numerical solution of population balance equations for nucleation growth and aggregation processes *Comp. & Chem. Eng.* 2007:31: 1576-1589.
- Singh, P. N., Ramkrishna, D., Kumar, S. Solution of population balance equation by MWR. *Comp. & Chem. Eng.* 1977: 23-31.
- Shah, B. H., Ramkrishna, D., Borwanker, J. D. Simulation of particulate systems using concept of the interval of quiescence. *AIChE J.* 1977:23: 897-904.
- Maisel, A., Kruis, F. E., Fissan, H. Direct Monte Carlo simulation of coagulation and aggregation. *J. of Aerosol. Sci.* 1999: 30: 417-418.
- Song, M., Qiu, X. J. Alternative to the concept of the interval of quiescence(IQ) in the Monte Carlo simulation of population balances. *Chem. Eng. Sci.* 1999: 54: 5711-5716.
- Kumar, S., Ramkrishna, D. On the solution of population balance equations by discretization-III. Nucleation, growth and aggregation of particles. *Chem. Eng. Sci.* 1997: 52: 4659-4679.
- Gunawan, R., Fusman, I., Braatz, R. D. High resolution algorithms for multidimensional population balance equations. *AIChE J.* 2004: 50: 2738-2749.
- Qamar, S., Elsner, M. P., Angelov, I., Warnecke, G., Seidel-Morgenstern, A. A comparative study of high resolution schemes for solving population balances in crystallization. *Comp. & Chem. Eng.* 2006: 30: 1119-1131.
- Qamar, S., Warnecke, G., Elsner, M. P. On the solution of population balances for nucleation, growth, aggregation and breakage processes. *Chem. Eng. Sci.* 2009: 64: 2088-2095.
- Chang, S. C. The method of space time conservation element and solution element-A new approach for solving Navier-Stokes and Euler equations. *J. of Comput. Phys.* 1995: 119: 295-324.
- Zhang, M., Yu, S. T., Chang, S. C. A Space-time conservation element and solution element method for solving the two-dimensional unsteady Euler equations using quadrilateral and hexedral meshes. *J. of Comput. Phys.* 2002: 175: 168-199.
- Qamar, S., Mudasser, S. On the application of a variant CESE method for solving two-dimensional MHD equations. *J. Appl. Num. Math.* 2010: 60: 587-696.
- Chang, S. C., Wang, X. Y., Chow, C. Y. New developments in the method of space-time conservation element and solution element-Applications to two-dimensional time-marching problems, NASA TM 106758, 1994.